# Magnetite pollution nanoparticles in the human brain

Barbara A. Maher[a,1], Imad A. M. Ahmed[b], Vassil Karloukovski[a], Donald A. MacLaren[c], Penelope G. Foulds[d], David Allsop[d], David M. A. Mann[e], Ricardo Torres-Jardón[f], and Lilian Calderon-Garciduenas[g,h]

[a]Centre for Environmental Magnetism and Palaeomagnetism, Lancaster Environment Centre, University of Lancaster, Lancaster LA1 4YQ, United Kingdom; [b]Department of Earth Sciences, University of Oxford, Oxford OX1 3AN, United Kingdom; [c]Scottish Universities Physics Alliance, School of Physics and Astronomy, University of Glasgow, Glasgow G12 8QQ, United Kingdom; [d]Division of Biomedical and Life Sciences, Faculty of Health and Medicine, University of Lancaster, Lancaster LA1 4YQ, United Kingdom; [e]Division of Neuroscience & Experimental Pyschology, School of Biological Sciences, University of Manchester, Manchester M6 8HD, United Kingdom; [f]Centro de Ciencias de la Atmósfera, Universidad Nacional Autónoma de México, Mexico City 04310, Mexico; [g]Neurotoxicology Laboratory, The University of Montana, Missoula, MT 59812; and [h]Universidad del Valle de México, Mexico City, 04850, Mexico

Edited by Yinon Rudich, Weizmann Institute of Science, Rehovot, Israel, and accepted by Editorial Board Member A. R. Ravishankara July 25, 2016 (received for review April 13, 2016)

**Biologically formed nanoparticles of the strongly magnetic mineral, magnetite, were first detected in the human brain over 20 y ago [Kirschvink JL, Kobayashi-Kirschvink A, Woodford BJ (1992) *Proc Natl Acad Sci USA* 89(16):7683–7687]. Magnetite can have potentially large impacts on the brain due to its unique combination of redox activity, surface charge, and strongly magnetic behavior. We used magnetic analyses and electron microscopy to identify the abundant presence in the brain of magnetite nanoparticles that are consistent with high-temperature formation, suggesting, therefore, an external, not internal, source. Comprising a separate nanoparticle population from the euhedral particles ascribed to endogenous sources, these brain magnetites are often found with other transition metal nanoparticles, and they display rounded crystal morphologies and fused surface textures, reflecting crystallization upon cooling from an initially heated, iron-bearing source material. Such high-temperature magnetite nanospheres are ubiquitous and abundant in airborne particulate matter pollution. They arise as combustion-derived, iron-rich particles, often associated with other transition metal particles, which condense and/or oxidize upon airborne release. Those magnetite pollutant particles which are <~200 nm in diameter can enter the brain directly via the olfactory bulb. Their presence proves that externally sourced iron-bearing nanoparticles, rather than their soluble compounds, can be transported directly into the brain, where they may pose hazard to human health.**

brain magnetite | magnetite pollution particles | Alzheimer's disease | combustion-derived nanoparticles | airborne particulate matter

Magnetic analyses of human brain samples have identified the presence of nanoparticles of magnetite, a strongly magnetic (ferrimagnetic) mixed $Fe^{2+}/Fe^{3+}$ iron oxide (1–3). Based on their nanoscale dimensions and euhedral (cubo-octahedral or prismatic) crystal shapes, these magnetite nanoparticles are thought to have formed by biological processes (1, 4), via in situ crystallization, possibly within the 8-nm-diameter cores of the iron storage protein, ferritin (e.g., ref. 5).

The specific presence of magnetite in the brain is important because it has been causally linked with potential cellular responses to external magnetic fields (e.g., in magnetic resonance imaging studies) (1), aging (6), and with neurodegenerative disease (e.g., refs. 2, 3, and 7). Previous work has shown a correlation between the amount of brain magnetite and the incidence of Alzheimer's disease (AD) (2, 3). Neuropathological changes associated with AD include the formation of senile plaques, containing β-amyloid fibrils (e.g., refs. 8, and 9). When associated with redox-active transition metal ions, such as $Fe^{2+}$ ions, β-amyloid can generate damaging reactive oxygen species, directly contributing to oxidative brain damage, a key early feature of AD (e.g., refs. 8–10). Magnetite nanoparticles have been found directly associated with AD plaques and tangles (e.g., refs. 11–13). In vitro experimental data show that magnetite acts synergistically to enhance the toxicity of β-amyloid (7).

We used magnetometry, high-resolution transmission electron microscopy (HRTEM), electron energy loss spectroscopy (EELS), and energy dispersive X-ray (EDX) analysis to examine the mineralogy, morphology, and composition of magnetic nanoparticles in and from the frontal cortex of 37 human brain samples, obtained from subjects who lived in Mexico City (14) (29 cases; ages 3 to 85 y; two females) and in Manchester, UK (8 cases; ages 62 to 92 y; five females; Tables S1 and S2). These brain magnetites display compelling similarity with the magnetite nanospheres formed by combustion, which are ubiquitous and prolific in urban, airborne particulate matter (PM) (15–19). We report here identification of the presence in human brain tissue of magnetite nanoparticles with an external, rather than an endogenous, source.

## Results

To quantify brain magnetic content, a cryogenic magnetometer was used to measure, at room and low temperature (77 K), the saturation magnetic remanence (SIRM) of frontal tissue samples, initially fresh-frozen and subsequently freeze-dried. The SIRM 77 K captures the magnetic contribution of ferrimagnetic grains that are so small (<~20 nm) as to be magnetically unstable (superparamagnetic) at room temperature. The magnetic brain particles were then examined directly, by HRTEM and EDX analyses both of ultrathin tissue sections and of magnetically extracted particles, after tissue digestion with the proteolytic

### Significance

We identify the abundant presence in the human brain of magnetite nanoparticles that match precisely the high-temperature magnetite nanospheres, formed by combustion and/or friction-derived heating, which are prolific in urban, airborne particulate matter (PM). Because many of the airborne magnetite pollution particles are <200 nm in diameter, they can enter the brain directly through the olfactory nerve and by crossing the damaged olfactory unit. This discovery is important because nanoscale magnetite can respond to external magnetic fields, and is toxic to the brain, being implicated in production of damaging reactive oxygen species (ROS). Because enhanced ROS production is causally linked to neurodegenerative diseases such as Alzheimer's disease, exposure to such airborne PM-derived magnetite nanoparticles might need to be examined as a possible hazard to human health.

Author contributions: B.A.M. designed research; B.A.M., I.A.M.A., V.K., and D.A.M. performed research; P.G.F. and D.A. contributed new reagents/analytic tools; B.A.M., I.A.M.A., V.K., D.A.M., D.M.A.M., R.T.-J., and L.C.-G. analyzed data; B.A.M. wrote the paper; D.M.A.M. provided brain tissue samples and medical diagnosis data; R.T.-J. provided airborne PM data; and L.C.-G. provided brain tissue samples.

The authors declare no conflict of interest.

This article is a PNAS Direct Submission. Y.R. is a Guest Editor invited by the Editorial Board.

[1]To whom correspondence should be addressed. Email: b.maher@lancaster.ac.uk.

This article contains supporting information online at www.pnas.org/lookup/suppl/doi:10.1073/pnas.1605941113/-/DCSupplemental.

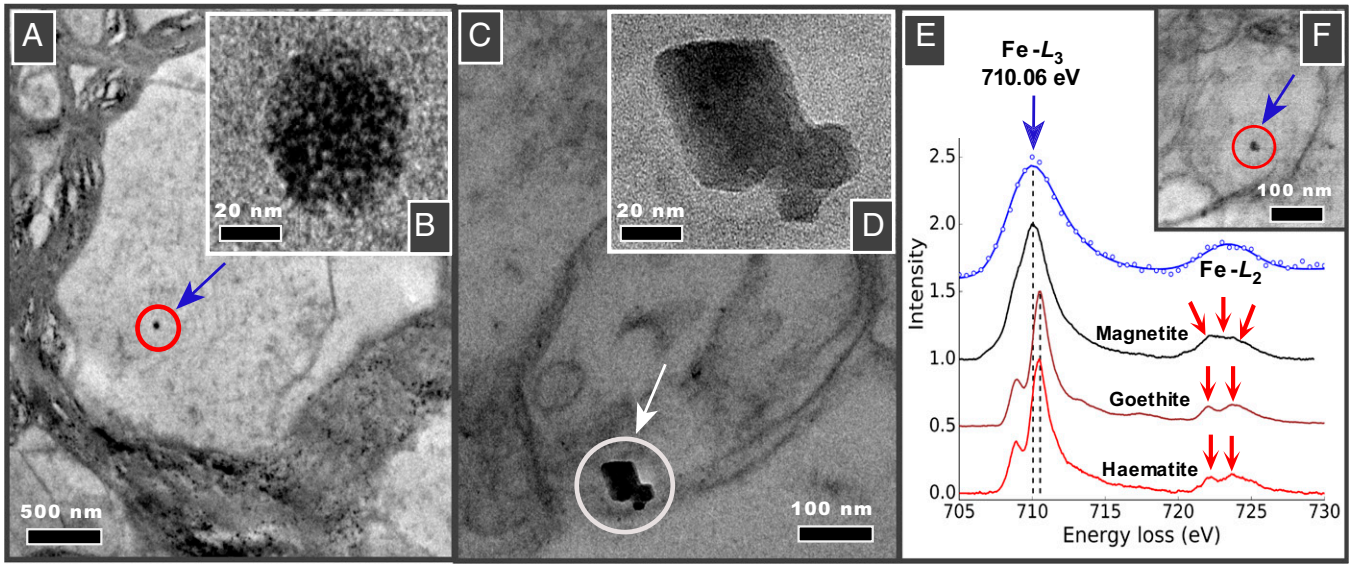


**Fig. 1.** Transmission electron micrographs of brain thin sections, identifying two distinct types of magnetite morphologies within frontal cells: (*A* and *F*) rounded particles (*A* shown at higher magnification in *B*); and (*C*) angular, euhedral particles, which we attribute to endogenous formation (particles from *C* shown at higher magnification in *D*). (*E*) EELS spectra (in blue) for the rounded particle shown in *F* and for standard iron oxide species. The position of the Fe–$L_3$ edge absorption peak, the broad feature of the Fe–$L_2$ (compared with the sharp edges, arrowed, of the fully oxidized $Fe^{3+}$ phases), and the integrated areas of the $L_3/L_2$ (5.5) and the Fe/O (0.56) are all consistent with magnetite (also see Figs. S3 and S4).

enzyme, papain. Every analytical step was designed and monitored to preclude any possible magnetic contamination.

The brain magnetic analyses identify the presence in all of the samples of strongly magnetic, easily magnetized nanoparticles, with concentrations ranging from 0.2 to 12 μg/g dry tissue (Fig. S1). The sample magnetic properties are dominated by behavior characteristic of interacting clusters of ferrimagnetic magnetite or maghemite (Fig. S2). Although highest brain magnetite concentrations (>10 μg/g dry tissue) are seen in many of the oldest cases, several of the much younger Mexico City cases, some exposed to high ambient concentrations of fine-grained (<2.5 μm aerodynamic diameter) airborne PM, also display high ferrimagnetic concentrations. Indeed, the highest brain magnetite content is found in a 32-y-old Mexico City resident (Fig. S1).

HRTEM and EELS analyses of the tissue sections identify the presence within frontal cells of magnetite, occurring as two distinct types of nanoparticle (Fig. 1 and Figs. S3 and S4). The majority of particles display rounded, even spherical morphologies (Fig. 1*A*, with higher magnification in Fig. 1*B*, and Fig. 1*F*), with diameters between 10 and 150 nm (Fig. S5). The additional presence in the brain cells of other transition metal nanoparticles, containing Pt, Ni, and Co (and possibly Cu), is identified by EELS (Fig. S6) and EDX (Figs. S7 and S8). These rounded magnetites contrast strongly with the angular, cubo-octahedral magnetite crystals also observed (relatively very rarely) within the brain tissue samples (Fig. 1*C*, and with higher magnification in Fig. 1*D*).

Crystallographic analysis of the particles within the tissue sections is difficult (due to rapid carbon buildup under the microscope electron beam). We therefore examined magnetically extracted (20) brain particles, to more fully characterize their mineralogy, surface textures, and particle size distribution. In accord with the observations on the untreated tissue samples, many of the extracted particles display rounded to spherical morphologies (Fig. 2 and Figs. S7–S10). In particular, some have fused surface crystallites (Fig. 2*H*) that would be very difficult to reconcile with low-temperature growth or dissolution formation processes. Indexing of the lattice fringes of the HRTEM of these particles is consistent with the magnetite crystal structure (Fig. 2 *C*, *E*, and *G*). Some surface oxidation toward its oxidized counterpart, maghemite, is evident (Fig. 2*I*). The particle size distribution of the rounded brain magnetite particles is notably broad, with a median (longest) diameter of 18 nm and maximum diameter of ∼150 nm (Fig. S5). Such dimensions greatly exceed those of nanoparticles formed within the 8-nm diameter of ferritin cores (5).

## Discussion

The geometric, angular particles resemble the in situ, biogenic magnetite previously reported (1, 4); we thus ascribe these euhedral magnetite particles to endogenous formation. The rounded magnetite nanoparticles (up to ∼150-nm diameter, with distinctive surface textures, and cooccurring with other PM-associated metals, including Pt) have not been identified previously in brain tissue sections. Apparently similar spherical structures, with diameters of 8 to 50 nm, have been found recently within amyloid plaque cores isolated from human brain (13) but were attributed to a biological rather than an external pollution-derived source. However, the surface textures, size, and size distribution of the spherical magnetites identified in our study, and the cooccurrence of PM-associated transition metal nanoparticles, are all inconsistent with the characteristics of biogenically formed magnetite (1, 4, 12). They bear compelling resemblance, instead, to the rounded/spherical magnetite nanoparticles (nanospheres) that are both ubiquitous and prolific within airborne, high-temperature (combustion-derived) PM (15–19, 21). The rounded shapes of these airborne, PM-derived magnetites (Fig. 3 and Fig. S11), and fusing of interlocking, surface crystallites (Fig. 3 *C* and *D*), reflect their high-temperature sources, and their subsequent crystallization, upon rapid cooling and/or oxidation, as Fe-rich nanospheres. Depending on PM source(s) (vehicular, subway, industrial, indoor), other transition metals are often coassociated with magnetite and other pollution nanoparticles (15–17, 19). Pt release, for instance, is associated with increasing vehicular use of catalytic converters (e.g., ref. 22). Frictional heating, e.g., of brake pads, can also produce high-temperature magnetite nanoparticles (21). Magnetite can arise from combustion of many types of organic matter, depending on heating temperature and atmosphere, and source Fe content (23–25).

Although PM mass has conventionally been used for setting of legislative airborne PM concentration limits, it is possible that

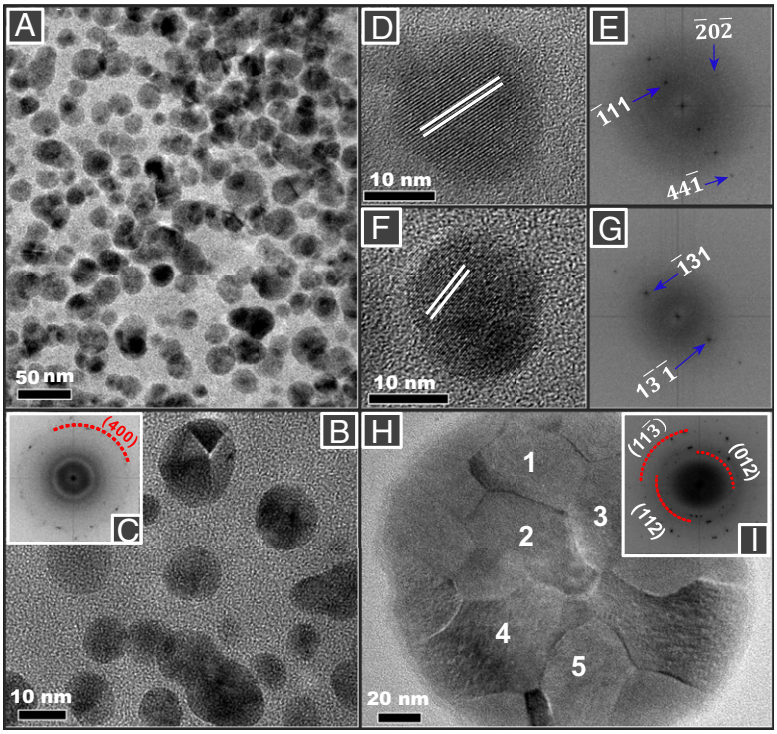


**Fig. 2.** Transmission electron micrographs of rounded particles magnetically extracted from human brain samples: (*A*, *D*, *F*, and *H*) Mexico City cases; (*B*) Manchester case. (*H*) A large (~150-nm diameter) spherical particle with fused, interlocking magnetite/maghemite surface crystallites. (*C*, *E*, and *G*) Indexing of the lattice fringes of the brain particles is consistent with the (400) reflection of magnetite and (*I*) mixed magnetite and maghemite of selected areas 1–5 in *H*.

ultrafine particle size and number are of greater significance in terms of mortality (26) and health impacts (e.g., ref. 27). Our magnetic measurements of roadside airborne PM [in Lancaster, United Kingdom (28)] indicate magnetite particle numbers equivalent to ~$2.01 \times 10^8$ $m^{-3}$ of roadside air, for ~50-nm-sized magnetite particles, for an ambient $PM_{10}$ concentration of ~40 $\mu g \cdot m^{-3}$ (compared, for example, with the annual mean $PM_{10}$ for Mexico City of between ~30 and 70 $\mu g \cdot m^{-3}$).

The abundant combustion-derived magnetite particles found in airborne PM can range widely in size, from less than 5 nm to more than 1 μm (15–17, 19). Those particles of nanoscale dimensions, requiring analysis by transmission rather than scanning electron microscopy, have, until recently, received less attention than the larger, often more heterogenous spherules. Magnetite nanospheres up to $\lesssim$ 200 nm can have a direct entry route to the brain through the axons of the olfactory nerve, as suggested by experimental studies on carbon (29) and $TiO_2$ nanoparticles (30), and the reported presence of NPs in the olfactory bulb of some Mexico City cases (14, 31–33).

Although many of the highly magnetic brain samples come from the older Manchester cases (>65 y at death), especially those with severe to moderate AD, equivalent or higher magnetite concentrations are also displayed by young (<40 y at death) Mexico City residents, especially those exposed to high $PM_{2.5}$ levels (annual mean $\gtrsim$25 $\mu g \cdot m^{-3}$). Increased metals content and AD neuropathological hallmarks have been found in young human brains exposed to high airborne $PM_{2.5}$ concentrations in Mexico City (14, 33). However, it was not previously known if the presence of metals in AD brains was due to transport to the brain of nanoparticles themselves or of their solubilized compounds. Our HRTEM results provide compelling evidence for the presence of externally sourced magnetite, and other metal-bearing nanoparticles in the frontal cortex of both the Mexico City and Manchester cases. It is notable that less than 5% of AD cases are directly inherited, indicating that nongenetic (environmental) factors, and/or gene/environment interactions, are likely playing a major role in initiating and/or promoting the disease. Jung et al. (34) found a 138% risk of increase of AD per increase of 4.34 $\mu g \cdot m^{-3}$ in $PM_{2.5}$ over a 9-y follow-up period in 95,690 individuals in Taiwan. It is not yet understood which PM properties (e.g., size, number, mineralogy, and associated chemical species) contribute most to toxic effects (e.g., ref. 35). Our preliminary magnetic results regarding both PM exposure and AD are thus both intriguing and warrant more intensive study. Because of their combination of ultrafine size, specific brain toxicity, and ubiquity

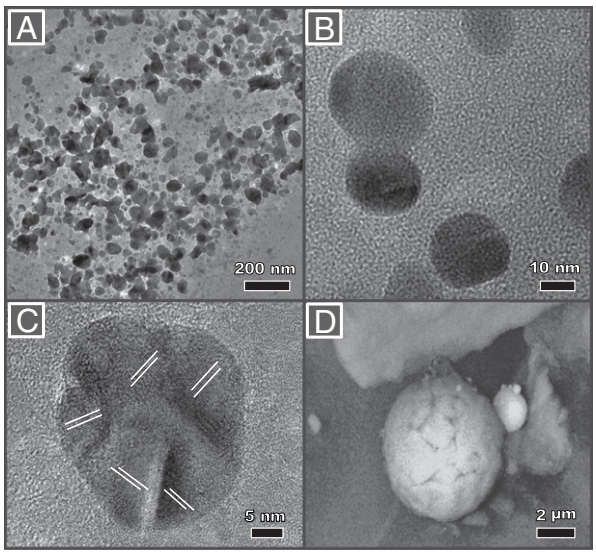


**Fig. 3.** TEM/scanning EM micrographs of anthropogenic (combustion-derived), magnetically extracted airborne particles. (*A*, shown at higher magnification in *B*) Magnetite nanoparticles from airborne PM (<10 μm), from Cable Street, Lancaster, United Kingdom (March 2009), sampled with a cascade impactor. Many particles display rounded profiles; some are fused together. (*C* and *D*) Spherical magnetite particles, Didcot power station, comprising fused magnetite particles (note the variable lattice orientations in *C* and the fused surface crystallites in *D*).

within airborne PM, pollution-derived magnetite nanoparticles might require consideration as a possible AD risk factor. In addition to occupational settings [including, for example, exposure to printer toner powders (36)], higher concentrations of magnetite pollution nanoparticles are likely to arise in the indoor environment from open fires (25) or poorly sealed stoves used for cooking and/or heating, and in the outdoor environment from vehicle (especially diesel) and/or industrial PM sources.

## Materials and Methods

**Brain Samples.** Fresh, frozen brain tissues were obtained from 38 individuals (Tables S1 and S2), 9 from the Manchester Brain Bank (ethical review and approval by the Manchester Brain Bank Management Committee and the Newcastle and North Tyneside I Regional Ethics Committee) and 29 from Mexico City, from forensic cases (fatal accidents) with no identifiable personal data, not meeting the regulatory definition of human subject research (University of Montana Institutional Review Board). A block (~25 g) of tissue was cut from the frontal lobes; subsamples were cut using nonmagnetic [polytetrafluoroethylene (PTFE)] instruments. The Manchester samples were dissected into gray (nine samples) and white (eight samples) matter.

To preclude any contamination, or operator bias, samples were handled with nonmagnetic instruments in a laminar flow clean bench environment and measured blind to diagnostics, and sample holder remanences were removed. The tissue samples were freeze-dried and placed in polystyrene sample holders (10 cc) for magnetic measurements.

**Magnetic Analyses.** Magnetic measurements were made at the Centre for Environmental Magnetism and Paleomagnetism, Lancaster University, using superconducting quantum interference device magnetometry. Room-temperature isothermal remanent magnetizations (IRMs) (Fig. S2*A*) were measured with a GM400 Cryogenic Magnetometer (mean background noise level 5.9 $\times 10^{-11}$ $A^2$; Cryogenic Consultants Ltd.); Low-temperature IRMs were measured (Fig. S2*B*) at temperatures between 293 and 77 K (±0.5 K) on a single-axis magnetic property measurement system XL magnetometer (Quantum Design). To identify magnetic grain sizes and/or magnetic interactions (37), anhysteretic remanence (ARM) was induced in a decaying (100 mT, peak) alternating magnetic field (af), with a small superimposed direct current (DC) field (0.08 mT), and subsequently af-demagnetized (Fig. S2*C*). Stepwise remanence acquisition was measured with incremental application of DC fields of 10, 20, 30, 50, 75, 100, and 300 mT and 1 T. The samples were cooled to 77 K and subjected to an applied DC field, 1 T, and their remanence was measured as they warmed to room temperature.

**Tissue Sections.**

***Magnetically extracted particles.*** A subset of samples (six tissue samples, and one blank without any tissue) was subjected to a magnetic extraction procedure, designed to maximize removal of submicrometer ferrimagnets (20). All reagents were prepared from ultrapurity Milli-Q water and prefiltered (<0.1 μm PTFE membrane filter) to preclude any particulate contamination; all instruments and sample holders were nonmagnetic (PTFE and polystyrene, respectively).

Papain from papaya latex (twice-crystallized; Sigma) was solubilized in 50 mM sodium acetate (prefiltered and magnetically measured multiple times to demonstrably preclude magnetic contamination). The tissue samples were digested overnight in papain at 65 °C and at fixed pH 7.0 ± 0.02, in a strictly oxygen-free environment inside a particulate-clean laboratory. The resultant suspension was circulated continuously (2 to 3 d, with a peristaltic pump) past a magnetized probe, producing a high field gradient at its tip (maximum field ~40 mT). The magnetically extracted particles were mounted on holey carbon films on carbon-coated copper grids for transmission electron microscopy (TEM).

***HRTEM, EELS, and EDX.*** Electron microscopy was conducted on two instruments, a JEOL ARM200cF and an FEI Tecnai F20, operated at 200 kV. A Gatan Quantum spectrometer was used for EELS in scanning TEM (STEM) mode. Due to rapid carbon buildup under the electron beam, only point acquisition spectra were collected; each spectrum typically summed from several spectra from each nanoparticle and from multiple nanoparticles. This procedure also minimized the electron dose experienced by individual nanoparticles and ensured that their chemical reduction was avoided. Time-dependent observations did not reveal any obvious structural or spectroscopic changes to the nanoparticles within the acquisition time (but were observed under prolonged exposure), and we conclude that the EELS data presented are representative of the nanoparticles' as-formed chemistry. EELS data were processed in Python using Hyperspy package. To determine dominant lattice spacings, fast Fourier transforms (FFTs) of high-resolution micrographs were compared with a simulated diffraction pattern of face-centered cubic magnetite (space group $Fd\bar{3}m$, no. 227, $a = 8.3941$ Å), and maghemite (space group $P4_332$, no. 212, $a = 8.3457$ Å). Sample sensitivity under STEM imaging precluded elemental mapping by EDX.

**ACKNOWLEDGMENTS.** We appreciate the reviewers' comments, which improved our manuscript. We thank Dr. Zabeada Aslam for her technical help, Dr. Mark Taylor (University of Lancaster) and Angelica Gonzalez-Maciel (Instituto Nacional de Pediatria, Mexico City) for assistance with tissue subsampling, and the University of Leeds Engineering and Physical Sciences Research Council-funded Nanoscience and Nanotechnology Facility for access to the HRTEM. We acknowledge the support of the Manchester Brain Bank by Alzheimer's Research UK and Alzheimer's Society through their funding of Brains for Dementia Research initiative, and service support costs from Medical Research Council.

1. Kirschvink JL, Kobayashi-Kirschvink A, Woodford BJ (1992) Magnetite biomineralization in the human brain. *Proc Natl Acad Sci USA* 89(16):7683–7687.
2. Pankhurst Q, Hautot D, Khan N, Dobson J (2008) Increased levels of magnetic iron compounds in Alzheimer's disease. *J Alzheimers Dis* 13(1):49–52.
3. Hautot D, Pankhurst QA, Khan N, Dobson J (2003) Preliminary evaluation of nanoscale biogenic magnetite in Alzheimer's disease brain tissue. *Proc Biol Sci* 270(Suppl 1): S62–S64.
4. Schultheiss-Grassi PP, Wessiken R, Dobson J (1999) TEM investigations of biogenic magnetite extracted from the human hippocampus. *Biochim Biophys Acta* 1426(1): 212–216.
5. Quintana C, Cowley JM, Marhic C (2004) Electron nanodiffraction and high-resolution electron microscopy studies of the structure and composition of physiological and pathological ferritin. *J Struct Biol* 147(2):166–178.
6. Dobson J (2002) Investigation of age-related variations in biogenic magnetite levels in the human hippocampus. *Exp Brain Res* 144(1):122–126.
7. Teller S, Tahirbegi IB, Mir M, Samitier J, Soriano J (2015) Magnetite-Amyloid-β deteriorates activity and functional organization in an in vitro model for Alzheimer's disease. *Sci Rep* 5:17261.
8. Allsop D, Mayes J, Moore S, Masad A, Tabner BJ (2008) Metal-dependent generation of reactive oxygen species from amyloid proteins implicated in neurodegenerative disease. *Biochem Soc Trans* 36(Pt 6):1293–1298.
9. Tabner BJ, Mayes J, Allsop D (2010) Hypothesis: Soluble Aβ oligomers in association with redox-active metal ions are the optimal generators of reactive oxygen species in Alzheimer's disease. *Int J Alzheimers Dis* 2011:546380.
10. Castellani RJ, et al. (2007) Iron: The redox-active center of oxidative stress in Alzheimer disease. *Neurochem Res* 32(10):1640–1645.
11. Collingwood J, Dobson J (2006) Mapping and characterization of iron compounds in Alzheimer's tissue. *J Alzheimer's Dis* 10(2-3):215–222.
12. Quintana C, et al. (2006) Study of the localization of iron, ferritin, and hemosiderin in Alzheimer's disease hippocampus by analytical microscopy at the subcellular level. *J Struct Biol* 153(1):42–54.
13. Plascencia-Villa G, et al. (2016) High-resolution analytical imaging and electron holography of magnetite particles in amyloid cores of Alzheimer's disease. *Sci Rep* 6: 24873.
14. Calderón-Garcidueñas L, et al. (2016) Prefrontal white matter pathology in air pollution exposed Mexico City young urbanites and their potential impact on neurovascular unit dysfunction and the development of Alzheimer's disease. *Environ Res* 146:404–417.
15. Mitchell R, Maher BA (2009) Evaluation and application of biomagnetic monitoring of traffic-derived particulate pollution. *Atmos Environ* 43(13):2095–2103.
16. Moreno T, et al. (2015) A new look at inhalable metalliferous airborne particles on rail subway platforms. *Sci Total Environ* 505:367–375.
17. Chen Y, Shah N, Huggins FE, Huffman GP (2006) Microanalysis of ambient particles from Lexington, KY, by electron microscopy. *Atmos Environ* 40(4):651–663.
18. Puffer JH, Russell EWB, Rampino MR (1980) Distribution and origin of magnetite spherules in air, waters, and sediments of the greater New York City Area and the North Atlantic Ocean. *J Sediment Petrol* 50(1):247–256.
19. Liati A, Pandurangi SS, Boulouchos K, Schreiber D, Dasilva YAR (2015) Metal nanoparticles in diesel exhaust derived by in-cylinder melting of detached engine fragments. *Atmos Environ* 101:34–40.
20. Hounslow MW, Maher BA (1996) Quantitative extraction and analysis of carriers of magnetization in sediments. *Geophys J Int* 124(1):57–74.
21. Kukutschová J, et al. (2011) On airborne nano/micro-sized wear particles released from low-metallic automotive brakes. *Environ Pollut* 159(4):998–1006.
22. Gómez B, Gómez M, Sanchez JL, Fernández R, Palacios MA (2001) Platinum and rhodium distribution in airborne particulate matter and road dust. *Sci Total Environ* 269(1-3):131–144.
23. Abdul-Razzaq W, Gautam M (2001) Discovery of magnetite in the exhausted material from a diesel engine. *Appl Phys Lett* 78(14):2018–2019.
24. Jordanova N, et al. (2006) Magnetism of cigarette ashes. *J Magn Magn Mater* 301(1): 50–66.
25. Mcclean RG, Kean WF (1993) Contributions of wood ash magnetism to archaeomagnetic properties of fire pits and hearths. *Earth Planet Sci Lett* 119(3):387–394.
26. Brunekreef B, Forsberg B (2005) Epidemiological evidence of effects of coarse airborne particles on health. *Eur Respir J* 26(2):309–318.
27. Pieters N, et al. (2015) Blood pressure and same-day exposure to air pollution at school: Associations with nano-sized to coarse PM in children. *Environ Health Perspect* 123(7):737–742.

28. Halsall CJ, Maher BA, Karloukovski VV, Shah P, Watkins SJ (2008) A novel approach to investigating indoor/outdoor pollution links: Combined magnetic and PAH measurements. *Atmos Environ* 42(39):8902–8909.
29. Oberdörster G, et al. (2004) Translocation of inhaled ultrafine particles to the brain. *Inhal Toxicol* 16(6-7):437–445.
30. Wang J, et al. (2008) Time-dependent translocation and potential impairment on central nervous system by intranasally instilled $TiO_2$ nanoparticles. *Toxicology* 254(1-2): 82–90.
31. Calderón-Garcidueñas L, et al. (2003) DNA damage in nasal and brain tissues of canines exposed to air pollutants is associated with evidence of chronic brain inflammation and neurodegeneration. *Toxicol Pathol* 31(5):524–538.
32. Block ML, Calderón-Garcidueñas L (2009) Air pollution: Mechanisms of neuroinflammation and CNS disease. *Trends Neurosci* 32(9):506–516.
33. Calderón-Garcidueñas L, et al. (2013) The impact of environmental metals in young urbanites' brains. *Exp Toxicol Pathol* 65(5):503–511.
34. Jung C-R, Lin Y-T, Hwang B-F (2015) Ozone, particulate matter, and newly diagnosed Alzheimer's disease: A population-based cohort study in Taiwan. *J Alzheimers Dis* 44(2):573–584.
35. Könczöl M, et al. (2011) Cytotoxicity and genotoxicity of size-fractionated iron oxide (magnetite) in A549 human lung epithelial cells: Role of ROS, JNK, and NF-κB. *Chem Res Toxicol* 24(9):1460–1475.
36. Gminski R, et al. (2011) Genotoxic effects of three selected black toner powders and their dimethyl sulfoxide extracts in cultured human epithelial A549 lung cells in vitro. *Environ Mol Mutagen* 52(4):296–309.
37. Maher BA (1988) Magnetic properties of some synthetic sub-micron magnetites. *Geophys J Int* 94(1):83–96.